Internal Tides in an Axially Symmetric Basin

KEUN-SIK LIM

Department of Oceanography, Naval Academy, Chin Hae 645-031, Korea

원통형 분지내의 내부조석

임 근 식

해군사관학교 해양학과

A new internal tide model for solving flow fields and wave generations is presented here which seems to be simple to apply, converges fast and yields accurate results. The new method employs a representation of vertical structure using dynamic basis functions which depend on the stratifications. The present method has been applied to the East Sea. For a constant Brunt-Väisälä case, weak baroclinic currents are generated over the entire continental slop; however, results using a more realistic stratification can be described using only the lowest modes and exhibit much more realistic behavior. Baroclinic tide generation is confined to the upper slope. Model results for the East Sea show the semi-diurnal baroclinic modes contain almost all the energy transferred from the barotropic mode.

내부파의 발생과 속도분포를 해결하기 위하여 새로운 내부조석 모델을 제시하였다. 이 새로운 방법은 해수의 성층화에 근거를 둔 역학적 함수의 수직구조를 이용하였다. 새로운 모델을 동해에 적용한 결과, 일정한 연직성층을 사용한 경우에는 약한 Baroclinic 해류가 전 대륙사면에서 발생되고, 보다 동해 해양조건에 맞는 해수의 성층화를 적용시키면 가장 낮은 모드만 사용하여서도 실제 해류분포를 나타나게 할 수 있다. 내부조석은 대륙사면의 상부에서 발생된다. 동해에서 반일주기의 내부조석은 첫 번째의 Baroclinic 모드로 보여지고, Barotropic 모드에서 전달된 거의 모든 에너지를 포함하고 있다.

INTRODUCTION

In recent years, interest in the margins of the continental shelves has increased as Oceanographers attempt to understand the interactions between the open sea and the shelf seas. The shelf areas are known to be dynamically active with enhanced current flows, large internal waves, internal tides, low frequency topographic waves, coastal upwelling and convective exchange. However, there is still much to be learned about the interactions between these phenomena and their impact on exchanges. There is thus a need to develop a more theoretical model and to observe individual processes.

This paper demonstrates a new model of the internal tide generation using normal mode. A number of different models have been presented for the calculation of internal tides generated by the interaction of the barotropic tide with large topographic features. The presence of internal tides with diurnal of semi-diurnal period has long been recognized, particularly near continental margins. These internal tides are believed to be induced by the interaction between the surface tide and topographic features.

Normal mode models have been used to examine the generation of internal tides. Sandstrom

(1976) constructed internal wave eigenfunctions for two dimensional topography to look at generation and coupling. Sandstrom compared his results with the Baines (1973) model and found good corespondance in baroclinic velocity components generated by a symmetrical cosine ridge.

Chaung and Wang (1981) used both ray tracing techniques and a two dimensional numerical model of internal tides over a continental slope. They compared the results of the two methods for constant and variable Brunt-Väisälä. They found good agreement between ray theory and numerical results.

Previous models using dynamic normal modes have been limited to small amplitude bottom topography due to use of common vertical structure functions for all locations. The present modal overcomes this difficulty by using local vertical structure functions and incorporating bottom coupling terms in the internal tide model.

The aims of this paper are (a) to provide solutions to the internal tide equation for a stratified fluid using local modal decomposition and (b) to apply the model to the East Sea for semi-diurnal frequencies so as to estimate the local significance of internal tides.

RESEARCH METHODS

1. Linearized Equations of Motion on an f-plane

The development of these equations is that of Reid (1988), though I have used cylindrical coordinates throughout in anticipation of applying the method to an axially symmetric basin. The starting equations are given in Gill (1982) as

$$\frac{1}{\rho}\frac{D\rho}{Dt} + \nabla \cdot u = 0 \tag{1}$$

and

$$\frac{Du}{Dt} + 2\Omega \times u = -\frac{1}{\rho}\nabla P - g + \nu \nabla^2 u + \nabla \Phi_T \tag{2}$$

where ρ is the potential density, u, the velocity, Ω, the Earth's angular rotation vector, P, the pressure, g, the local gravitational acceleration, ν, the kinematic viscosity, and Φ_T, the tide potential. Eq. (1) and (2) are simplified by assuming an inviscid fluid, non-divergent flow, no advection of velocity, no horizontal stratification and imposing the hydrostatic approximation. If the potential density for the rest state is ρ_o with maximum potential density ρ_m, and the hydrostatic pressure for the rest state is $P_o(z)$ then the following definitions may be made

$$p = \frac{P - P_o(z)}{\rho_m}$$

$$b = -\frac{g(\rho - \rho_o(z))}{\rho_m}$$

and

$$N^2 = -\left(\frac{g}{\rho_m}\right)\frac{\partial \rho_o}{\partial z}$$

where p is the kinematic pressure anomaly. b is the buoyancy term, and N is the Brunt-Väisälä frequency. Using cylindrical coordinates with the above assumptions, (1) and (2) become

$$\frac{\partial b}{\partial t} + N^2 w = 0 \tag{3}$$

and

$$\frac{\partial u}{\partial t} - fv + \frac{\partial p}{\partial r} = \frac{\partial \Phi_T}{\partial r} \tag{4}$$

$$\frac{\partial u}{\partial t} + fu + \frac{1}{r}\frac{\partial p}{\partial \theta} = \frac{1}{r}\frac{\partial \Phi_T}{\partial \theta} \tag{5}$$

$$\frac{\partial p}{\partial z} - b = 0 \tag{6}$$

The boundary condition for the top of the water column is taken to be a material surface, for which

$$w = \frac{1}{g}\frac{\partial p}{\partial t} \quad \text{at } z = 0 \tag{7}$$

while the boundary at the sea bed is a solid surface with free flow along it,

$$w = -u \cdot \nabla h \quad \text{at } z = -h \tag{8}$$

Boundary conditions at the center and outer edge of the basin will be considered later. The geometry of the basin and forcing is such that the equations are periodic in θ and t. Combining conservation of mass, (3), with conservation of vertical momentum, (6), yields

$$W = -\frac{1}{N^2}\frac{\partial}{\partial t}\frac{\partial p}{\partial z} \qquad (9)$$

Substituting (9) into the equation of continuity yields

$$\frac{\partial u}{\partial r} + \frac{1}{r}\frac{\partial v}{\partial \theta} - \frac{\partial}{\partial t}\frac{\partial}{\partial z}\left(\frac{1}{N^2}\frac{\partial p}{\partial z}\right) = 0 \quad (10)$$

The boundary conditions (7) and (8) can similarly be reduced to

$$\frac{1}{N^2}\frac{\partial p}{\partial z} = -\frac{p}{g} \quad \text{at } z = 0 \qquad (11)$$

and

$$\frac{1}{N^2}\frac{\partial}{\partial t}\frac{\partial p}{\partial z} = u \cdot \nabla h \quad \text{at } z = -h \qquad (12)$$

Dynamic normal modes are now introduced to solve the governing equations developed above for a stratified fluid. The vertical structure of pressure and horizontal velocity can be represented as a sum of modal pressures and velocities multiplied by the local vertical structure function, $F_n(z)$. The local vertical structure function can be defined by solving the Sturm-Liouville(S-L) problem as Flierl (1978) does

$$\frac{\partial}{\partial z}\left(\frac{1}{N^2(z)}\frac{\partial F_n}{\partial z}\right) + \lambda_n F_n = 0 \qquad (13)$$

subject to the boundary conditions

$$\frac{\partial F_n}{\partial z} = \frac{-N^2}{g}F_n \quad \text{at } z = 0 \qquad (14)$$

and

$$\frac{\partial F_n}{\partial z} = 0 \quad \text{at } z = -h \qquad (15)$$

2. Coupled Normal Mode Equations

Because the basis functions F_n are a complete

orthonormal set, p and u can be represented as

$$p(r,\theta,z,t) = \sum_{n=0}^{\infty} p_n(r,\theta,t)F_n(z,h) \qquad (16)$$

$$u(r,\theta,z,t) = \sum_{n=0}^{\infty} u_n(r,\theta,t)F_n(z,h) \qquad (17)$$

where,

$$p_n = \frac{1}{h}\int_{-h}^{0} pF_n dz \qquad (18)$$

and

$$u_n = \frac{1}{h}\int_{-h}^{0} uF_n dz \qquad (19)$$

To determine predictive equations for p_n and u_n, (4) through (5) and (10) are multiplied by F_n and integrated over z making use of (18) and (19) to get

$$h\frac{\partial u_n}{\partial t} + hf\hat{n}_z \times u_n + \int_{-h}^{0} F_n\nabla p dz = h\nabla\Phi_T\delta_{n0} \qquad (20)$$

and

$$\frac{\partial}{\partial t}\int_{-h}^{0} F_n\frac{\partial}{\partial z}\left(\frac{1}{N^2}\frac{\partial p}{\partial z}\right)dz$$

$$-\int_{-h}^{0} F_n\nabla \cdot u dz = 0 \qquad (21)$$

Note that the tidal forcing is multiplied by δ_{n0}, indicating it acts only on the barotropic mode. This fact arises because the tide forcing is taken to be independent of depth and the baroclinic F_n have a zero vertical integral. Eq. (16) and (18) are used to simplify the pressure gradient term in (20) as below,

$$\int_{-h}^{0} F_n\nabla p dz = \sum_m \int_{-h}^{0} F_n\nabla(p_m F_m)dz$$

$$= h\nabla p_n + \sum_m p_m\int_{-h}^{0} F_n\nabla F_m dz \qquad (22)$$

Now,

$$\nabla F_m = \frac{\partial F_m}{\partial h}\nabla h \qquad (23)$$

and a non-dimensional topographic coupling matrix S_{nm} can be defined

$$S_{nm}' = \int_{-h}^{0} F_n \frac{\partial F_m}{\partial h} dz \qquad (24)$$

Using (24), the momentum equation (20), is now

$$\frac{\partial u_n}{\partial t} + f_{\hat{z}} \times u_n + \nabla p_n = -\frac{1}{h} \sum_{m=0}^{\infty} p_m S_{nm}(\nabla h)$$

$$+ \nabla \Phi_T \delta_{n0} \qquad (25)$$

Likewise (16) becomes

$$\lambda_n \frac{\partial p_n}{\partial t} + \frac{1}{h} \nabla \cdot (h u_n) = \frac{1}{h} \sum_{m=0}^{\infty} S_{mn} u_m \cdot (\nabla h) \qquad (26)$$

The matrix S_{nm}, defined by the integral relation (24), can be evaluated in closed form for known λ and $F_n(z, h)$.

$$S_{nm} = \frac{1}{2} \delta_{nm} + \left(\frac{\lambda_n - \lambda_m}{\lambda_m} - 2\delta_{nm} \right)^{-1} (F_n F_m)_{-h} \qquad (27)$$

Details may be found in Lim (1989).

3. Transform of Modal Equations to the Frequency Domain

For sustained forcing at frequency ω, the solutions for complex u_n, v_n, and p_n will also be of simple harmonic form proportional to $\exp(i(\omega t + l\theta))$. Therefore $\partial/\partial t$ can be replaced by $i\omega$ and $\partial/\partial \theta$ by il so that (25) to (26) become

$$i\omega u_n - f v_n + \frac{dp}{dr} + \frac{1}{h} \sum_{m=0}^{M} p_m S_{nm} \frac{dh}{dr} = \frac{gA}{R} \delta_{n0}, \quad (28)$$

$$i\omega v_n + f u_n + \frac{il}{r} p_n = i \frac{gAl}{R} \delta_{n0}, \qquad (29)$$

and

$$i\omega\lambda_n p_n + \frac{1}{rh} \frac{d}{dr}(rh u_n) + \frac{il}{r} v_n$$

$$- \frac{1}{h} \sum_{m=0}^{M} u_m S_{mn} \frac{dh}{dr} = 0. \qquad (30)$$

Eq. (29) is a purely algebraic relation between u_n, v_n, and p_n. It can be solved for v_n to yield

$$v_n = i \frac{f}{\omega} u_n - \frac{1}{\omega r} \left(p_n - gA \frac{r}{R} \delta_{n0} \right) \qquad (31)$$

It is also convenient to solve the equations in te-

rms of volume transport rather than velocity. The modal volume transport Q_n is defined by the relation

$$u_n = iQ_n/rh. \qquad (32)$$

Substituting (31) and (32) into (28) through (30) gives the following governing equations for p_n and Q_n

$$\frac{dp_n}{dr} = -\frac{f}{\omega} \frac{1}{r} p_n + \left(\omega - \frac{f^2}{\omega} \right) \frac{Q_n}{rh} - \frac{1}{h} \sum_{m=0}^{M}$$

$$p_m S_{nm} \frac{dh}{dr} + \frac{gA}{R} \left(1 + \frac{fl}{\omega} \right) l^2 \delta_{n0} \qquad (33)$$

and

$$\frac{dQ_n}{dr} = \frac{f}{\omega} \frac{1}{r} Q_n - \left(\omega\lambda_n - \frac{l^2}{\omega r^2} \right) rh p_n$$

$$+ \frac{1}{h} \sum_{m=0}^{M} Q_m S_{mn} \frac{dh}{dr} - \frac{gA}{R} \frac{l^2 h}{\omega} \delta_{n0}. \qquad (34)$$

Direct forcing by the tide potential occurs only for the barotropic mode the baroclinic modes are excited by coupling to the barotropic mode and other baroclinic modes via the coupling matrix, S, in the presence of bottom slope, dh/dr.

4. Inner and Outer Boundary Conditions

If an impermeable wall exists at the basin perimeter, $r = R$, then the condition there is simply $Q_n = 0$(or $u_n = 0$ if $h \neq 0$) for all modes. Under this condition total reflection occurs for every mode. For an *inviscid* model such as this one, a simple way of providing this sink is to radiate energy at $r = R$ into a hypothetical reservoir that allows mass to flow in either direction but returns no energy. Therefore, a possible generalized condition is

$$c_n u_n = \gamma_n p_n \quad \text{at } r = R \qquad (35)$$

where γ_n is a non-dimensional admittance for mode n which must satisfy $\gamma_n \geq 0$, and $C_n = \lambda_n^{-1/2}$. The energy flux into the hypothetical sink is proportional $(Rh\gamma_n/c_n)\Gamma_n^2$ which the energetics subsection will show is never negative. In terms of Q_n, condition (35) is equivalent to
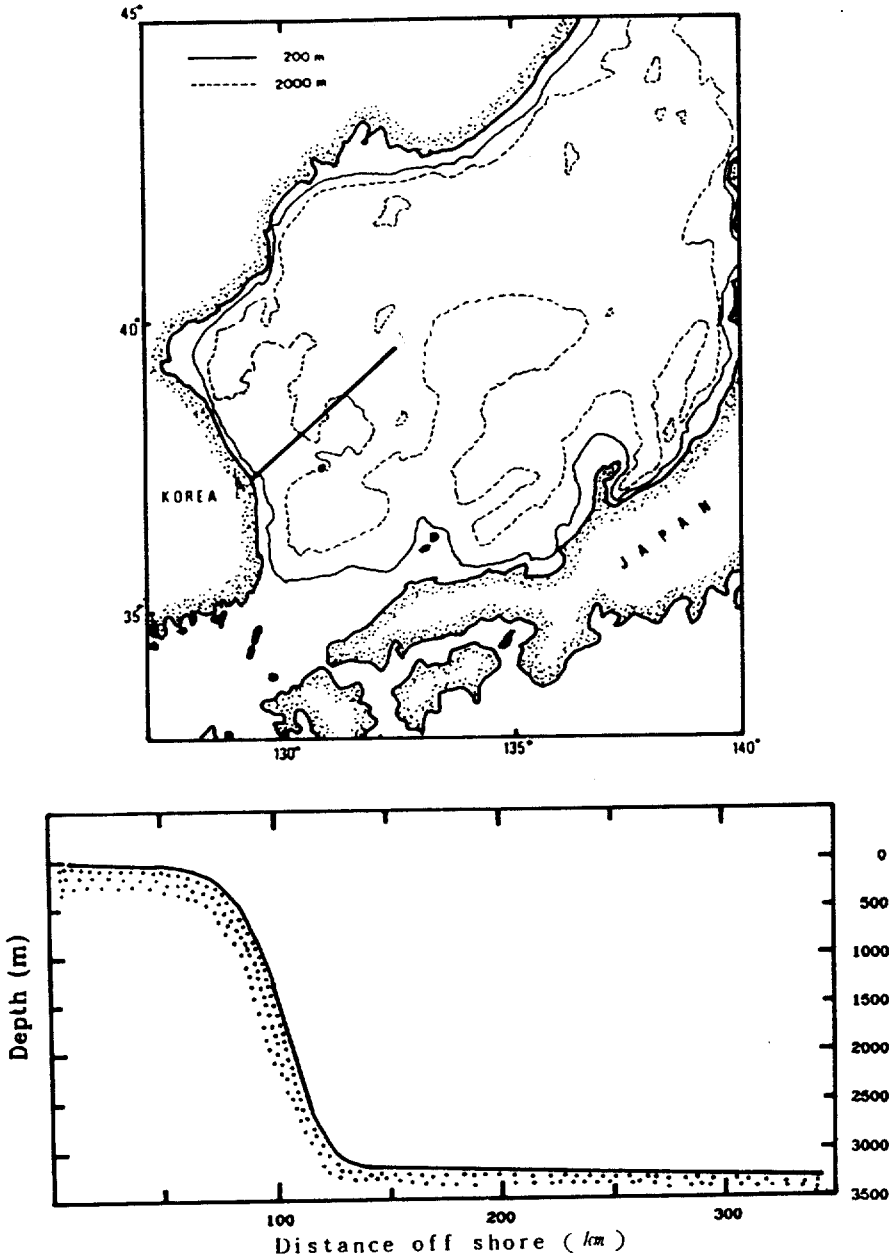
Fig. 1. Bathymetry of the East sea.

$$Q_n = -i\Gamma_n p_n \quad \text{at} \quad r = R \tag{36}$$

where $\Gamma_n = Rh(R)\gamma_n/c_n$. The case of an impermeable wall for mode n is simply $\Gamma_n = 0$.

A second boundary condition involving p_n or Q_n is required at or near $r=0$. For forcing by the tide potential with $\omega^2 \neq f^2$ and $l^2 \neq 0$, (33) and

(34) require that p_n and Q_n vanish at $r=0$ if their derivatives are to be finite.

The governing equations (33) and (34) then require the following single relation between these derivatives at $r=0$:

$$\frac{dp_n}{dr} - \frac{gA}{R}\delta_{n0} = \frac{(\omega - fl)}{h}\frac{dQ_n}{dr} \tag{37}$$

Table 1. Bathymetry fitting coefficients for all model runs.

b_0	2.9957
b_1	0.03665/10³
b_2	1.7392
m	0.02256/10³
x_1	50 km from shore
x_2	135 km from shore

A practical boundary condition for numerical calculation can then be found from (37) to be

$$p_n - gA\frac{r_0}{R}\delta_{n0} = \frac{(\omega - fl)}{h} Q_n \qquad (28)$$

at $r = r_0$, the innermost grid point, where $\lambda_n \omega^2 r_0^2 \ll 1$.

RESULTS AND DISCUSSION

The size of the basin, bathymetry, latitude and forcing are chosen to reflect conditions on the East Sea shelf and slope. The radius of the basin is 350 km, which gives it the same scale as the East Sea, and the latitude is taken as 37° N. The depth is specified as a piecewise continuous function of the distance from shore with three regions: a narrow shallow sloping shelf, a steep escarpment and a deep constant depth abyssal plain. Fig. 1 shows the bathymetry over the three regions of the basin.

The actual form of the analytic functions specifying depth was determined by a best fit for an alongsore averaged section over the East Sea shelf with the fitting formula given below:

$$h = \begin{cases} \exp(b_0 + b_1 x), \text{ for } 0 < x < x_1, \\ \exp(b_0 + b_1 x + b_2 \sin(m(x - x_1))^2), \\ \quad \text{for } x_1 < x < x_2, \text{ and} \\ h(x_2), \text{ for } x_2 < x \end{cases} \qquad (39)$$

where $x = R - r$, the distance from shore, and b_0, b_1, b_2, m, x_1, and x_2, are given in Table 1. These coefficients with (39) give a minimum shelf depth of 20 m and a maximum abyssal depth of 3000 m.

The forcing for the M_2 tide in the East Sea is primarily through the astronomical tide generating force (ATGF) rather than tidal currents through the Korean strait and Tsugaru strait. Accordingly, the forcing period of the model is taken to be that of the M_2 tide, 12.42 hrs. The direction
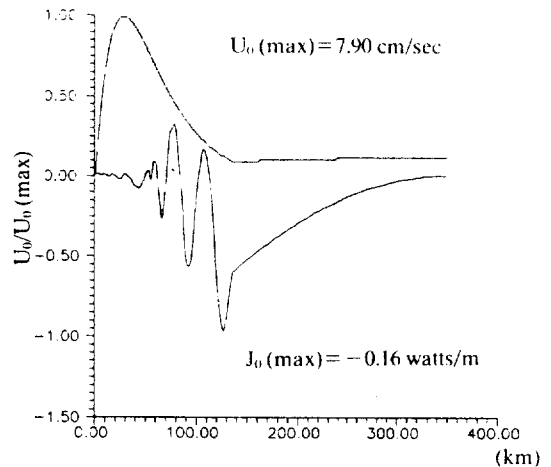

Fig. 2. Barotropic energy flux and U-velocity for variable stratification.

of phase propagation is taken as counterclockwise. The amplitude of the tidal forcing is determined by the ATGF strength with the Earth tides taken into account.

The number of grid points was chosen as 500 in order to provide a minimum grid resolution of approximately ten grid points per wavelength for the most limiting case, which was dependent on the Brunt-Väisälä frequency on the shelf and the maximum number of modes examined. This number of grid points was retained for other model runs for the sake of uniformity.

The model output consists of real and imaginary values of transport Q_n and kinematic pressure anomaly p_n. From these values the real and imaginary modal velocities in the r and θ directions, U_n and V_n are back calculated. The magnitudes of U_n and V_n are plotted as a function of r. From U_n, V_n and p_n, modal energy fluxes and the transfer of energy from barotropic to baroclinic modes are plotted as a function of r.

In all model runs the barotropic model showed similar behavior as shown in Fig 2 and 3. The radial velocity U_0 was almost zero near the open ocean. It increased rapidly over the continental slope and shelf and decreased to zero within 100 km of the shore boundary. The phase of U_0 remained locked at 90°. At 100 km offshore both for uniform stratification and for variable stratification the model show U_0 to be around 2 cm/s,
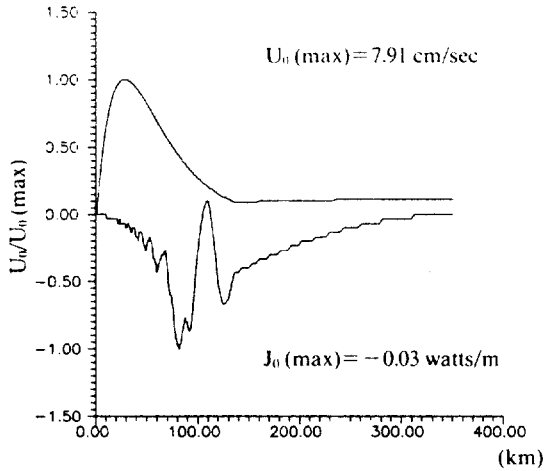
U_0 (max) = 7.91 cm/sec

J_0 (max) = −0.03 watts/m

(km)

Fig. 3. Barotropic energy flux and U-velocity for uniform stratification.

Table 2. Comparison of 4 and 6 baroclinic modes for uniform stratification.

modes	4 modes	6 modes
U_0(max)	7.91 cm/sec	7.90 cm/sec
J_0(max)	0.03 watts/m	0.03 watts/m
U_1(max)	25.7 cm/sec	19.3 cm/sec
J_1(max)	0.02 watts/m	0.02 watts/m
U_2(max)	6.70 cm/sec	23.8 cm/sec
J_2(max)	0.02 watts/m	0.02 watts/m
U_3(max)	45.2 cm/sec	13.0 cm/sec
J_3(max)	0.02 watts/m	0.04 watts/m
U_4(max)	70.2 cm/sec	45.2 cm/sec
J_4(max)	0.02 watts/m	0.11 watts/m

and at 50 km offshore U_0 is about 7.9 cm/s. These values are only approximate due to the dependence of the exact magnitude of U_0 in the model on the stratification chosen. The energy flux, J_0, is zero at the center of the basin and decreases to a minimum at the slope. Most of the decrease occurs over the slope region. The stratification is one of the factors which determines the strength of the bottom coupling. Strong bottom coupling decrease the amplitude of U_0 more the cases of weakly coupled or pure barotropic ones. However, the shope of the velocity curves remains steady and the reduction in amplitude is on the order of 20% indicating most of the energy remains in the barotropic mode.

Preliminary studies were made using a constant Brunt-Väisälä frequency of 2.5 cph. This value of Brunt-Väisälä frequency was based on a typical change in density from the surface to 3000 m in the East Sea and thus represents an average over the entire water column. The constant Brunt-Vä isälä frequency case trivializes the solution of the Sturm-Liouville problem for the vertical structure functions. For this case, the F_n become cosine fu-nctions with a normalized bottom value of $\pm\sqrt{2}$. This simplifies the calculations and shortens the run time immensely. However, in addition to being unrealistic, the choice of a constant N has another big problem. This problem is is that many

higher modes are very energetic, meaning that the representation of velocity and pressure with depth can not be truncated to just a few modes. Because of the stringent grid resolution requirements which increased both run time and the dimensions of stored arrays, the choice was made to use a maximum of only six baroclinic modes.

Comparisons of runs for four and six baroclinic modes for uniform stratification are shown in Table 2. Table 2 brings out the differences between the four and six baroclinic modes. The observation that a large number of modes is needed to represent the velocity and pressure fields is consistent with previous studies such as that of Rattray, Dworski, and Kavala (1969) who used 100 normal modes to represent the internal waves field in their study. For example, Chuang and Wang (1981) used eleven normal modes to specify the boundary conditions in their numerical scheme. The energetic higher modes present in this model are consistent with the previous studies, but this is speculation in light of the few baroclinic modes investigated.

Fig 4. shows the velocities for the uniform stratification using four baroclinic modes. Strong bottom coupling from barotropic to baroclinic modes occurs over the entire slope with less intense coupling over the shelf. Shoreward modal energy fluxes show oscillations at their internal wavelengths. These oscillations are strongest over the slope and decay rapidly (with about five wavelength) over the shelf. All baroclinic modes an energy flux into the shoreward boundary as a consequence of the
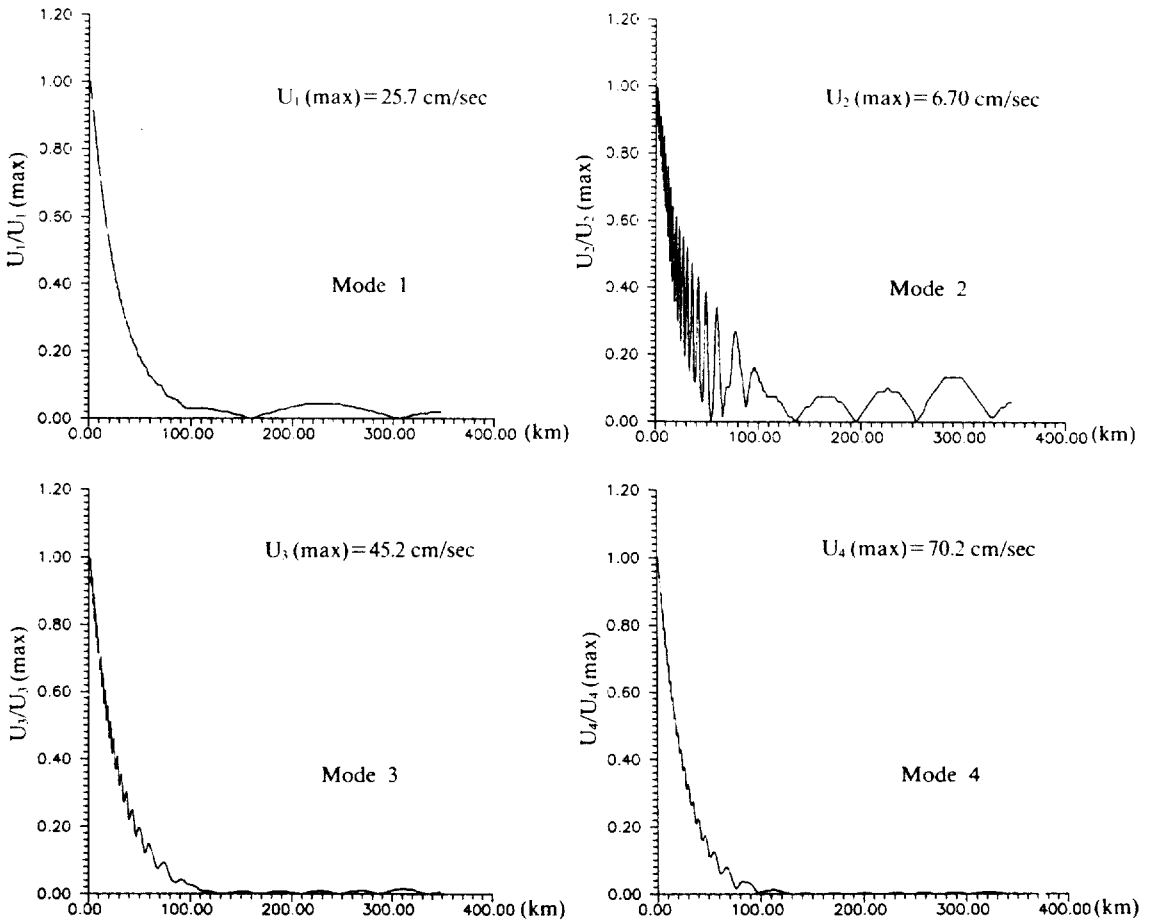
Fig. 4. U-velocities of 4 baroclinic modes for uniform stratification.

radiational boundary condition. For the case of uniform stratification, internal tide generation is weak and many baroclinic modes are highly energetics as shown in Fig. 4.

A second set of model runs was performed with a variable stratification. This stratification was chosen to resemble that found in the East Sea. The East Sea does not have a deep wind mixed layer and is strongly stratified near the surface during summer and autumn. The stratification decreases from a high of about 12 cph at 50 m to about 0.5 cph at 500 m. Below 500 m it varies slowly between 0.5 and 0.2 cph.

The uniform stratification over the shelf allowed the bottom values of the vertical structure functions to be specified as $\pm \sqrt{2}$ over much of the shelf. The actual form of the base state stratifica-

Table 3. Stratification parameters. N_0 is chosen to give the actual density change over z, and other parameters are chosen such that the density change over the entire water column is equal to that in the East Sea.

N_0	8.41 cph
N_b	0.5 cph
r	$1/210 \, m^{-1}$
z_1	125 m

tion is given below:

$$N(z) = \begin{cases} N_0, & \text{for } 0 < z < z_1, \text{ and} \\ (N_0 - N_b) \exp(r(z_1 - z)) + N_b, & \text{for } z_1 < z \end{cases} \quad (40)$$

with the numerical values for coefficients given in Table 3.
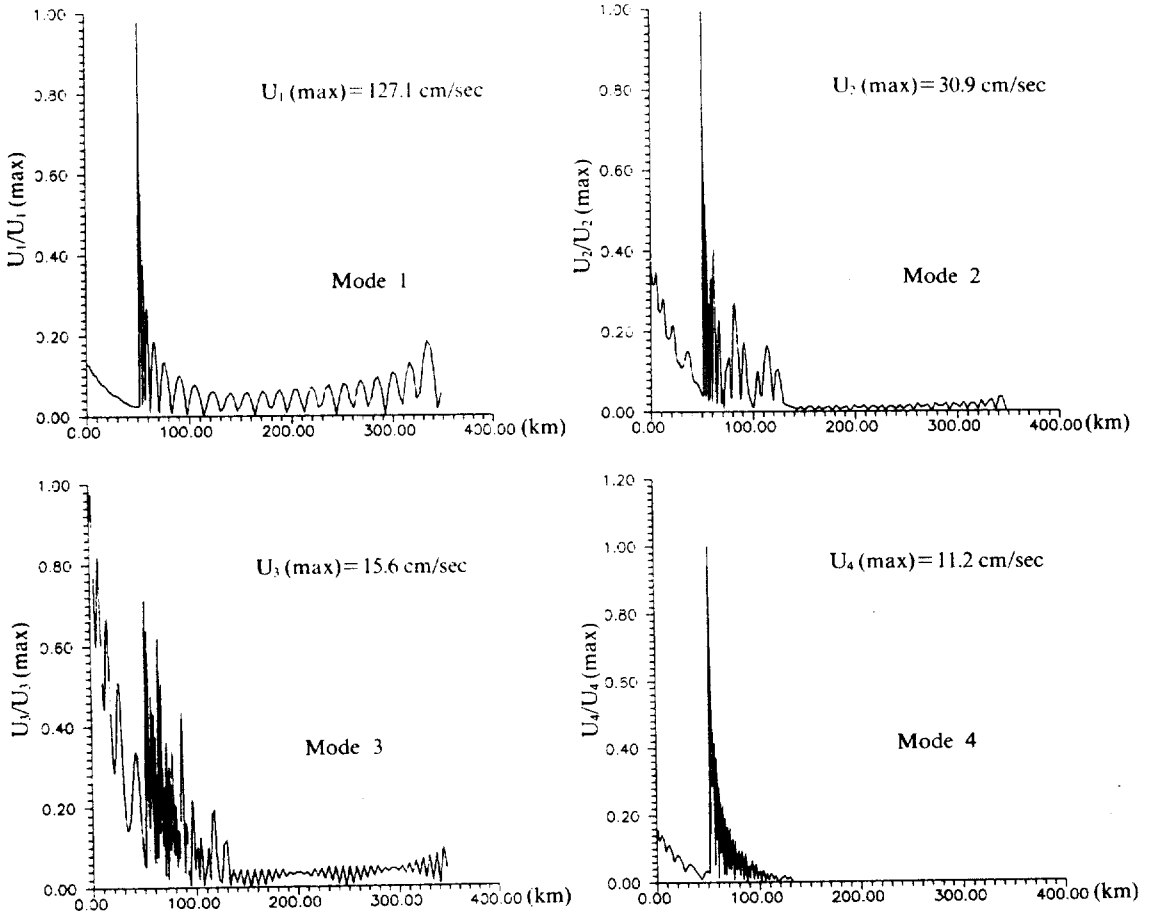
By using this statification, I examined the effect

Fig. 5. U-velocities of 4 baroclinic modes for variable stratification.

Table 4. Comparison of 4 and 6 baroclinic modes for variable stratification.

modes	4 modes	6 modes
$U_0(max)$	7.90 cm/sec	7.90 cm/sec
$J_0(max)$	0.16 watts/m	0.02 watts/m
$U_1(max)$	127.1 cm/sec	80.5 cm/sec
$J_1(max)$	0.09 watts/m	0.02 watts/m
$U_2(max)$	30.9 cm/sec	7.10 cm/sec
$J_2(max)$	0.01 watts/m	0.004 watts/m
$U_3(max)$	15.6 cm/sec	7.70 cm/sec
$J_3(max)$	0.014 watts/m	0.003 watts/m
$U_4(max)$	11.2 cm/sec	9.40 cm/sec
$J_4(max)$	0.01 watts/m	0.001 watts/m

of varying statification over the slope, where bottom coupling is strong. In contrast to the case of uniform Brunt-Väisälä frequency, results of mo-

del runs using four and six baroclinic modes are nearly identical. Table 4 shows how close the velocities and energy fluxes are. The lowest baroclinic modes are highly energetics. This indicates the lowest baroclinic modes contain almost all the energy transferred from the barotropic mode. The fact that most of the energy is contained in the lowest modes for the more realistic stratification is consistent with previous results reported by Wunsch (1975).

Fig. 5 shows the velocities for the adopted non-uniform stratification using four baroclinic modes. In contrast to the case of uniform stratification, where U_n-velocity is strong over the entire slope, baroclinic velocities show that the strongest topographic coupling occurs only over the upper slope
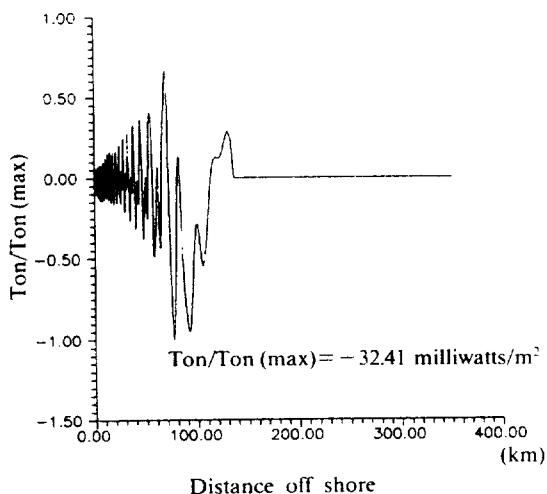
Fig. 6a. Transfer of energy from barotropic to baroclinic modes for uniform stratification.

Fig. 6b. Transfer of energy from barotropic to baroclinic modes for variable stratification.

for the variable stratification. It is in this region where both the bottom slope and stratification are large.

This result is in agreement of modelling studies of Baines (1982) and Chuang and Wang (1981) who found that baroclinic energy was concentrated at the upper slope for non -uniform stratification. It is also in agreement with measurements reported by Huthnance and Baines (1982) on the shelf-slope break off the northwest coast of Africa.

Fig. 6 illustrates that net energy transfer from the barotropic to baroclinic modes was also much weak for the case of uniform stratification. One reason for this is that the bottom coupling is weaker over most of the slope for uniform case. Another is that reconversion from baroclinic to barotropic energy occurs over a region of the lower slope between about 100 km and 135 km from the coast region. The stronger transfer of energy from barotropic to baroclinic modes is also reflected in the strength of the baroclinic currents of the non-uniform case when compared to the uniform.

Baroclinic velocity maxima in Table 4 are comparable to and sometimes even stronger than the barotropic velocity maximum. For the non-uniform case, the mode one velocities had a maximum of 127.1 cm/sec at the continental break. The
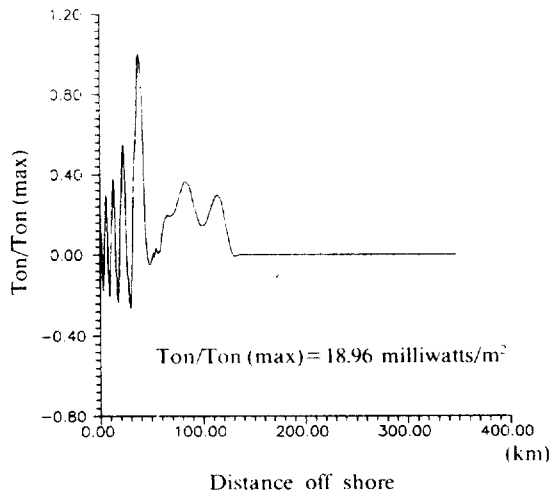
relative phases of the baroclinic currents also rotated over the course of one internal wavelength. It is important to remember that the first mode velocity must be multiplied by the local vertical structure function is of order one over the water column, meaning that the mode one magnitude does give a good indication of the depth dependent velocity over the shelf.

CONCLUSIONS

I have presented a new algorithm for the numerical solution of a class of coupled internal tide problems. The model presented in this study is shown to produce several results.

1. Previous models using normal modes have several shortcoming for calculation of internal tides generated by the interaction of the barotropic tide with large topographic features, and have been limited to small amplitude bottom topography due to use of common vertical structure functions for all locations. The present model overcomes this difficult by using coupling matrix. This modal model should be seen as complementary to previous internal tide models. By using a time stepping scheme and uniform grid, the model can be applied to arbitrary two dimensional topography.

2. The present model has been applied to the

East Sea. For the case of uniform stratification, internal tide generation is weak and many baroclinic modes are highly energetics. Topographic coupling occurs over the entire continental slope. With a more realistic variable stratification, the first internal mode contains almost all of the baroclinic energy. Topographic coupling is both weaker and confined to the upper continental shelf. Model results for the East Sea show the semi-diurnal baroclinic tide to be primarily mode one and strong relative to the barotropic.

Future extensions of this and any other internal tide generation model should attempt to incorporate nonlinear terms and viscosity. The generation and dissipation of internal tides is thought to be a highly nonlinear process.

REFERENCES

Baines, P.G., 1973. The generation of internal tides by flat-bump topography. *Deep-Sea Res.*, **20**: 179-205.

Baines, P.G., 1982. On internal tide generation models. *Deep-Sea Res.*, **29**: 307-338.

Chuang, W.S. and D.P. Wang, 1981. Effects of density front on the generation and propagation of internal tides. *J. Phys. Oceanogr.*, **11**: 1357-1374.

Flierl, G.R., 1978. Models of vertical structure and the calibration of two-layer models. *Dynamics of Atmospheres and Oceans*, **2**: 341-381.

Gill, A.E., 1982. Atmosphere-Ocean Dynamics. Academic Press Inc., 662 pp.

Huthnance, J.M. and P.G. Baines, 1982. Tidal currents in the northwest African upwelling region. *Deep-Sea Res.*, **29**: 285-306.

Lim, K.S., 1989. The shelf wave eigenvalue problem for a stratified ocean. Ph. D. Dissertation, Texas A & M university, 107 pp.

Rattray, M., J.G. Dworski and P.E. Kavala, 1969. Generation of long internal waves at lthe continental slope. *Deep-Sea Res.*, **16**: 179-195.

Reid, R.O., 1988. Forced tides in a stratified circular basin with r-dependent depth, unpublished manuscript, Texas A & M University, 33 pp.

Sandstrom, H., 1976. On topographic generation and coupling of internal waves. *Geophys. Fl. Dyn.*, **7**: 231-270.

Wunch, C., 1975. Internal tides in the ocean. *Rev. Geophys. Space. Phys.*, **13**: 167-182.